Spin crossover behaviour in a homologous series of iron(II) complexes based on functionalized-bipyridyl ligands

Journal:	*Inorganic Chemistry*
Manuscript ID	ic-2018-00850p.R1
Manuscript Type:	Article
Date Submitted by the Author:	n/a
Complete List of Authors:	Xue, Shufang; Universite catholique de Louvain, Institute of Condensed Matter and Nanosciences Guo, Yunnan; Universite catholique de Louvain, Institute of Condensed Matter and Nanosciences Rotaru, Aurelian; Stefan cel Mare University of Suceava, Faculty of Electrical Engineering and Computer Science Müller-Bunz, Helge; UCD, School of Chemistry and Chemical Biology Morgan, Grace; University College Dublin, School of Chemistry & Chemical Biology Trzop, Elzbieta; Universite de Rennes 1, Institut de Pysique de Rennes - Physics Collet, Eric; Institut de Physique de Rennes, Physics Olah, Julianna; Budapest University of Technology and Economics Garcia, Yann; Université Catholique de Louvain, Institute of Condensed Matter and Nanosciences

Spin crossover behaviour in a homologous series of iron(II) complexes based on functionalized-bipyridyl ligands

Shufang Xue,[†] Yunnan Guo,[†] Aurelian Rotaru,[‡] Helge Müller-Bunz,[§] Grace G. Morgan,[§] Elzbieta Trzop,[ǁ] Eric Collet[ǁ], Julianna Oláh [□] and Yann Garcia[†,*]

[†]Institute of Condensed Matter and Nanosciences, Molecules, Solids and Reactivity (IMCN/MOST), Université catholique de Louvain, Place L. Pasteur 1, 1348 Louvain-la-Neuve, Belgium

[‡]Department of Electrical Engineering and Computer Science & MANSiD Research Center, "Stefan cel Mare" University, University Street, 13, Suceava 720229 Romania

[§]School of Chemistry, University College Dublin, Belfield, Dublin 4, Ireland

[ǁ]Univ Rennes 1, CNRS, Institut de Physique de Rennes, UMR 6251, UBL,

35042 Rennes, France

[□]Department of Inorganic and Analytical Chemistry, Budapest University of Technology and Economics, H-1111 Szent Gellért tér 4. Budapest, Hungary

ABSTRACT: A series of bulky substituted bipyridine-related iron(II) complexes $[Fe(H_2Bpz_2)_2(L)]$ (pz = pyrazolyl) were prepared, where L = 5,5'-dimethyl-2,2'-bipyridine (**bipy-CH_3**, **1**), L = dimethyl-2,2'-bipyridyl-5,5'-dicarboxylate (**MeObpydc**, **2**), L = diethyl-2,2'-bipyridyl-5,5'-dicarboxylate (**EtObpydc**, **3**), L = diisopropyl-2,2'-bipyridine-5,5'-dicarboxylate (***i*-PrObpydc**, **4**). The crystal structures of five new iron(II) complexes were determined by X-ray diffraction: the one of **1, 3** and **4** as well as two modifications of **3** (**3B**) and **4** (**4B**). Complexes **1** and **3B** display incomplete spin crossover (SCO) behavior due to a freezing-in effect whereas **3** and **4B** undergo gradual and incomplete SCO behaviors. Complexes **2** and **4** show a completely gradual and steep SCO, respectively. Such different SCO behaviors can be attributed to electronic substituent effect in bipyridyl ligand conformation and crystal-packing effect. Importantly, the electronic substituent effect of the isopropyl acetate group and C-H···O supramolecular interactions in **4** contribute to a highly cooperative behavior, which leads to an abrupt thermally induced spin transition.

INTRODUCTION

Spin crossover (SCO), a spin-switching phenomenon that may exist in $3d^4$–$3d^7$ transition metal complexes, is regarded as a fascinating field of investigation finding echo in as diverse potential applications such as ultra-high-density memory devices, sensors, molecular electronics and spintronics.[1] Such outstanding and useful physical property is due to the switching between the low-spin (LS) and high-spin (HS) states in a reversible, detectable and controllable fashion by the action of external stimuli (temperature, pressure, light irradiation and chemical decoration). The switching can be accompanied by drastic changes in the magnetic properties (diamagnetism-paramagnetism), but also with some physical response such as structural, vibrational, dielectric, and optical properties.[2] Until now, the majority of SCO materials involve spin carriers surrounded by different organic ligands with various morphologies. In order to realize potential applications, the properties referring to an abrupt and complete signal response[3] with a hysteresis[4] around room temperature are considered as very important requirements. One efficient approach results from the fine-tuning the ligand field around the metal center as well as the control of supramolecular interactions (crystal packing effects) between switching units, thus justifying the use of crystal engineering concepts. Bipydine (**bipy**) is considered as a classical representative of imine ligands for SCO systems.[5] The spin nature of these complexes lies in the high σ-donor power of the imine function and the empty, low-lying π orbitals of the ligand molecules. Therefore an effective strategy to tune the ligand field strength of **bipy** complexes into the crossover range consists in modifying the σ-donor or π-acceptor character.[5] From the standpoint of organic synthesis, it was thought to substitute the **bipy** ligand at the C_3, C_4, C_5 and C_6 positions, to explore the impact of the electronic substituent effect and crystal packing on the SCO properties. Substituents at the C_3,[6] and C_6,[7] positions have a strong influence on the iron spin-state, as well as on steric and electronic grounds. Conversely, provided that the substituents are at positions relatively remote from the donor atoms (C_4 and C_5), no significant change occurs in the ligand field strength as well as on the $[FeN_6]^{2+}$ core.[8],[9] One exception is the occurrence of “spin equilibrium” in the Fe^{II} complex of 5,5’-diethylcarboxylate-2,2’-bipyridine.[8]

As the archetype of bipy-related SCO systems, the mononuclear complex $[Fe(H_2Bpz_2)_2(L)]$ (pz = pyrazolyl, L = **bipy**) was found to exhibit a thermally induced

SCO transition at 160 K,[10] also with pressure[11] and light irradiation.[12] Since then, successive efforts have concentrated on the modification of the **bipy** ligand, involving for instance a diarylethene photoisomerizable unit for ligand driven light induced spin change.[13] An interdigitated aromatic donor group to allow strong π···π interactions in the crystal lattice of mononuclear iron(II) complexes was also introduced.[14] Hydrophilic alkyl tails were also added to improve the spin-transition temperature via nanosphere organization.[15] A strong electron-donating amino group was also recently introduced.[16] Amazingly, protonation of the amino group in $[Fe(H_2Bpz_2)_2(\mathbf{bipy\text{-}NH_2})]$ (**bipy-NH$_2$** = 4,4'-diamino-2,2'-bipyridine) displays spectacular enhancement of $T_{1/2}$ from 160 K to 297 K, allowing operating SCO around room temperature.[16] Notwithstanding these representative examples, the investigation of structure–property relationships is at the heart of the SCO field to reach a full control of magnetic properties. Aiming, herein, at shedding light on the SCO influence of bipy substituents, we have designed a series of bulky substituted bipy-ligands at C_5 and $C_{5'}$ positions (Scheme 1), and assembled Fe^{II} complexes **1**-**4**. Hopefully, the central skeleton of FeN_6 was found similar to the original crystal arrangement around the Fe^{II} center[10], which allows meaningful comparisons. Due to the electronic substituent effect and crystal-packing effect, the SCO behavior drastically differs from complexes to complexes: **1** and **3B** displays incomplete SCO behavior, **2** shows a gradual SCO whereas **3** and **4B** undergo gradual and incomplete SCO behaviors. Importantly, the combination between electronic substituent effect of the isopropyl acetate group and C-H···O interactions in **4** provide relatively high cooperativity, which leads to an abrupt SCO behavior.

Scheme 1. Fe^{II} complexes based on a series of bulky substituted bipy-ligands at C_5 and C_5' positions

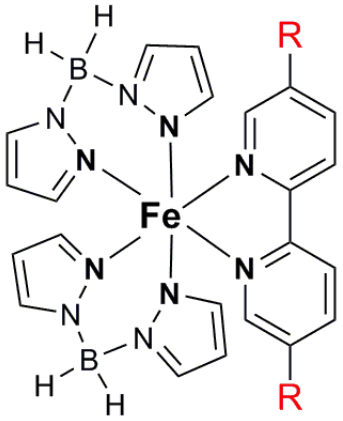

R = -CH_3 (**bipy-CH_3, 1**)
R = -$COOCH_3$ (**MeObpydc, 2**)
R = -$COOCH_2CH_3$ (**EtObpydc, 3**)
R = -$COOCH(CH_3)_2$ (***i*-PrObpydc, 4**)

2. RESULTS

2.1. Synthesis and General Characterization. The bipy-type ligands (Scheme 1), 2,2′-bipyridine-5,5′-dicarboxylic acid (**bpydc**),[17] dimethyl-2,2'-bipyridyl-5,5'-dicarboxylate (**MeObpydc**),[18] diethyl-2,2'-bipyridyl-5,5'-dicarboxylate (**EtObpydc**)[19] and diisopropyl-2,2'-bipyridine-5,5'-dicarboxylate (***i*-PrObpydc**)[20] were prepared following literature procedures. Powder samples for **1**-**4** were prepared by similar procedures described in the literature (Scheme 2).[10]

Scheme 2. Synthetic procedure for the bulky substituted bipy ligands (**bipy-CH_3**, **MeObpydc**, **EtObpydc** and ***i*-PrObpydc)** and the iron (II) complexes (**1**-**4**).

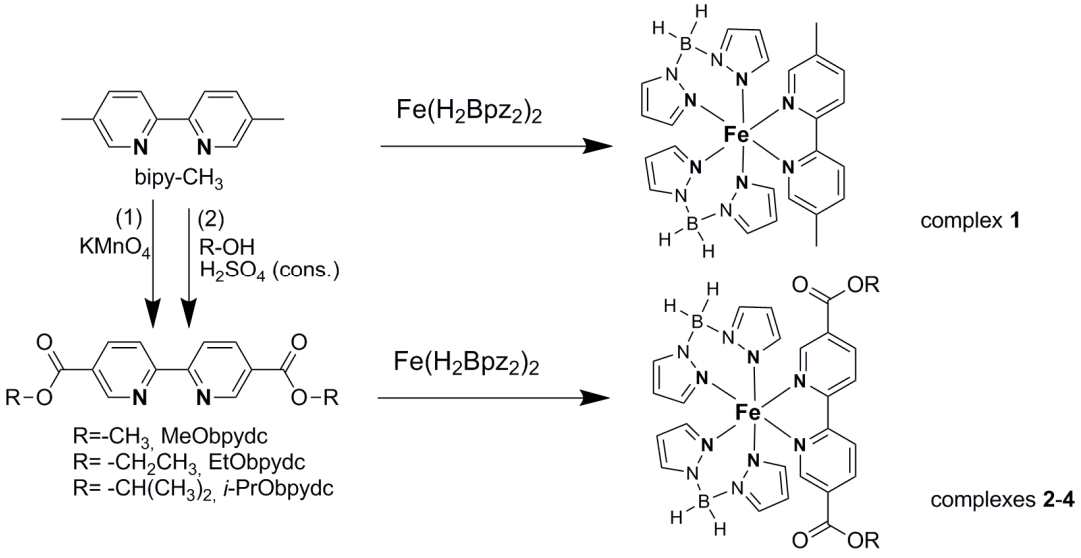

Single crystal of **1** was obtained by slow diffusion in MeOH under $Ar_{(g)}$, using a single-tube glass vessel. The **bipy-CH_3** in CH_3OH was placed on the top of a $Fe(H_2Bpz_2)_2$ methanolic solution. Given to the different solubility, single crystals of **3** and **4** were obtained by slow diffusion in methanol/dichloromethane mixture under

$Ar_{(g)}$ using a single-tube glass vessel. The bipyridine dicarboxylate (**MeObpydc**, **EtObpydc** or ***i*-PrObpydc**) in CH_2Cl_2 was placed on the bottom of a methanolic solution containing $Fe(H_2Bpz_2)_2$. Pink-violet single crystals for **1** and dark green bulk crystals for **3** and **4**, namely **3B** and **4B** formed after one week. Of particular interest was that needle crystals of **3** and **4** were observed after one night. Attempts to crystallize **2** failed due to the poor solubility of **MeObpydc** ligand, yielding systematically to a solid crystalline product despite numerous varied reaction conditions. All these complexes were successfully characterized by elemental analysis, mass spectra analysis (MS), thermogravimetric analysis (TGA), Fourier-transform infrared spectroscopy (FTIR), differential thermal analysis (DSC), single-crystal X-ray diffraction, magnetic susceptibility measurements and ^{57}Fe Mössbauer spectroscopy. The crystal structures of all the complexes except **2** were determined by single-crystal X-ray diffraction at variable temperatures. Details for the structure solution and refinement are summarized in Table S1 and selected bond distances and angles are listed in Table S2. Importantly, no lattice solvent molecules were detected neither by crystallography nor by TGA (Figure 1). The thermal stability of complexes **1**-**4** was found very high, above 500 K for **1** and **4**, or slightly below for **2** and **3**. FTIR analysis revealed that all the complexes have a similar coordination mode irrespective of the **bipy**-type ligand around the iron(II) centre (Figure S1).

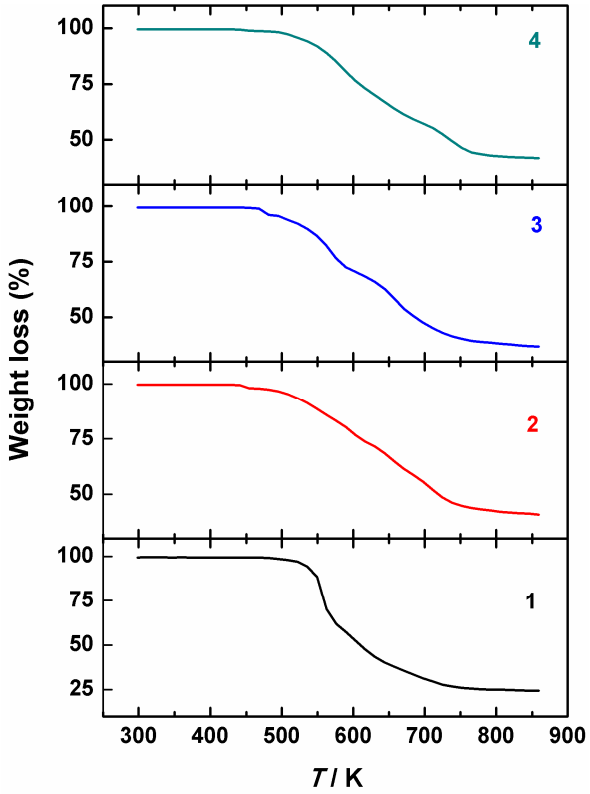

Figure **1**. TGA profile for powder samples **1**-**4** performed under a $N_{2(g)}$.

2.2. X-ray crystallography

Crystal structure of 1. Complex **1** crystallizes in the monoclinic $P2_1/c$ space group with the formula $[Fe(H_2Bpz_2)_2(\mathbf{bipy\text{-}CH_3})]$. A perspective view of the molecular structure of **1** at 95 K is represented in Figure 2. The whole molecule consists of one bidentate **bipy-CH$_3$** group and two $(H_2Bpz_2)^-$ anions coordinated to Fe^{II} in *cis* mode. The Fe-N bond lengths are in the range of 2.150(2)-2.240(2) Å which is consistent with HS Fe^{II}. The *cis* angles of the iron(II) coordination sphere range from 74.62(9) to 98.38(9)°, and the octahedral distortion parameter (Σ) is found to be 50.7°. Although a FeN_6 core is identified, which matches the one of the reference complex $[Fe(H_2Bpz_2)_2(bipy)]$ (**5**),[9] a comparison of the bond distances in **1** and **5** (Figure S2) shows considerable differences in the ligand field strength, thus leading to different magnetic behaviors (*vide infra*). The crystal packing also shows some differences with weaker π···π interactions between the adjacent bipy ligands in **1** than that in **5** (Figure S3).

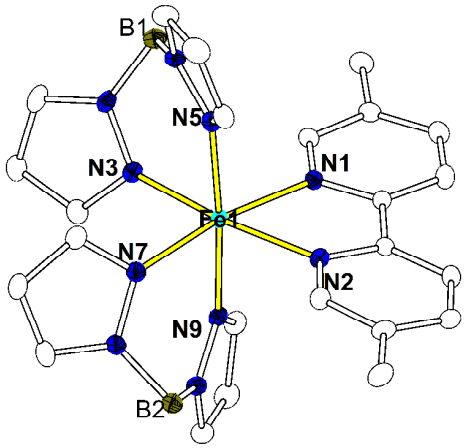

Figure 2. Perspective view of the molecular structure of **1** at 95 K. Displacement ellipsoids are drawn at the 30% probability level and H atoms were omitted for the sake of clarity.

Careful inspection of the packing arrangement (Figure S3) reveals a 2D supramolecular structure which is organized *via* weak C-H···π intermolecular interactions (C3-H3···centroid and C11-H11B···centroid distance: 2.513 Å and 2.828 Å) from the **bipy-CH$_3$** ligand to a pyrazolyl moiety. Attempts to collect data at 20 K after detecting a spin state crossover below 90 K from magnetic measurements (see Figure 12), reveals the Fe-N bond length is still larger than 2.1 Å (Table S2). In this case, X-ray crystallography is limited for spin detection given the low amount of spin carriers involved in the SCO process (ca. 10% as found by ^{57}Fe Mössbauer spectroscopy, *vide infra*). The HS state could also result from flash cooling of the crystals from room temperature by our He cryostream at 20 K which may trap the HS state, as observed on another example by X-ray diffraction.[21]

Crystal structures of 3 and 4. In order to avoid the occurrence of transesterification (*vide infra*), crystal growth was carried out overnight with the corresponding ligand-containing dichloromethane solution into a methanolic solution of Fe(H_2Bpz$_2$)$_2$ leading to X-ray quality crystals of **3** and **4** of [Fe(H_2Bpz$_2$)$_2$(**EtObpydc**)] and [Fe(H_2Bpz$_2$)$_2$(***i*-PrObpydc**)], respectively (Figures 3 and 4).

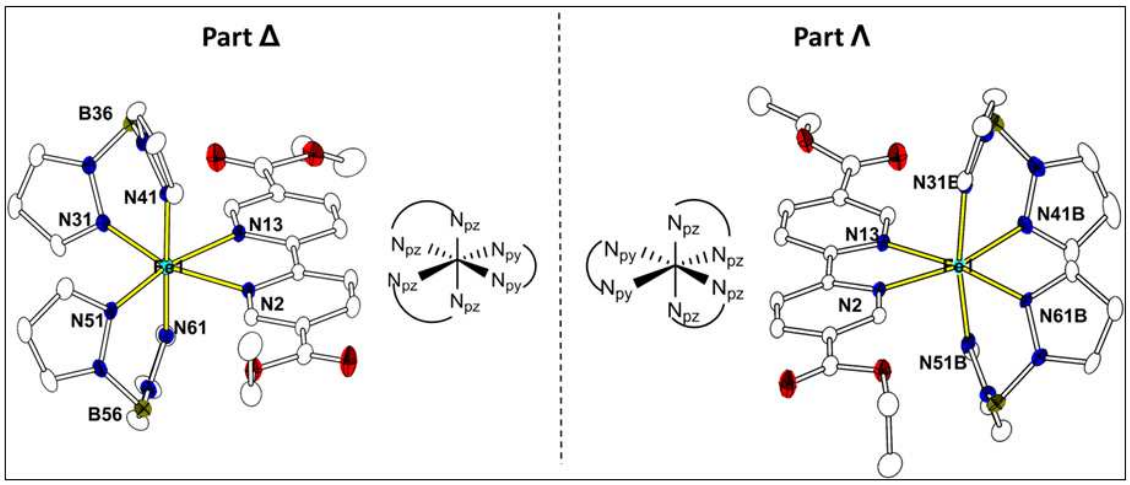

Figure 3. Perspective view of the molecular structures of enantiomers in **3** at 296 K. Displacement ellipsoids are drawn at the 10% probability level and the H atoms have been omitted for the sake of clarity.

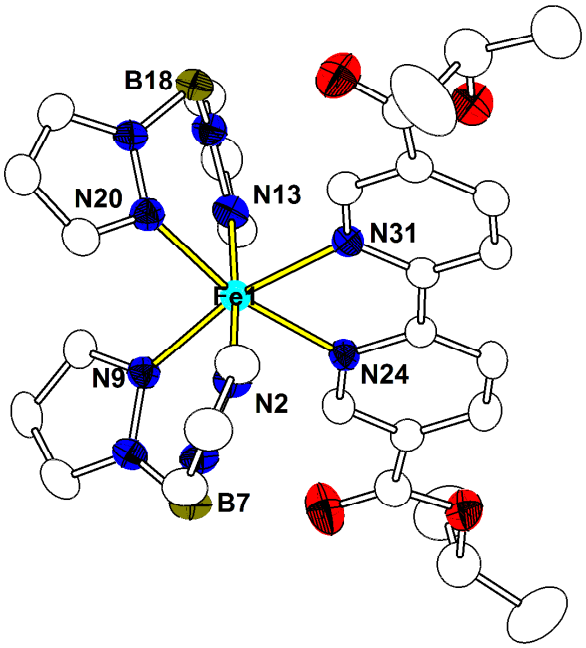

Figure 4. Perspective view of the molecular structures of **4** at 297 K. Displacement ellipsoids are drawn at the 30% probability level and the H atoms have been omitted for the sake of clarity.

X-ray crystallographic analysis at both high (296 K) and low temperatures (92 and 20 K) reveals that **3** shows a significant disorder of the boron containing pyrazolyl ligand, denoted as Part Δ and Part Λ, which are enantiomers (Figures 3 and S4). The

disorder can be viewed as being generated by applying a mirror plane along the **EtObpydc** ligand or perpendicular to it. All Fe^{II} ions are in a distorted FeN_6 octahedral coordination environment derived from one **EtObpydc** ligand and two $(H_2Bpz_2)^-$ anions. Comparison of structural data at different temperatures reveals that the average Fe-N_{pz} bond length variation is $\Delta R \sim 0.135$ Å in Part Δ whereas in Part Λ, the mean value $\Delta R < 0.055$ Å (Table S2). Such considerable reorganization of molecular geometry corresponds to a temperature-driven spin transition in Part Δ. Careful inspection of the packing arrangement reveals a 1D supramolecular chain generated by short interligand C-H···O contacts (C28-H28···O1*, symmetry code:*, -1+x, y, 1+z, Table S3) within the complex units (Figure 5).

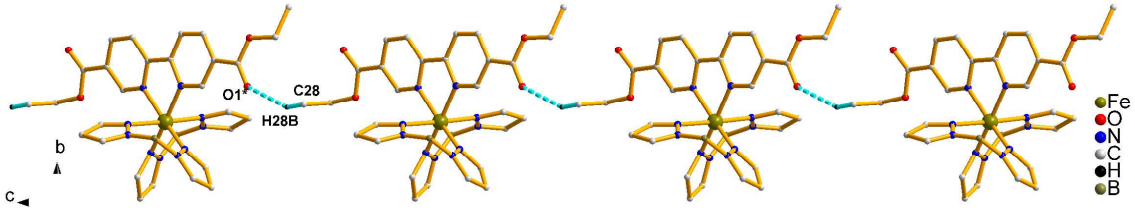

Figure 5. Crystal packing for **3** showing intermolecular C-H···O interactions (C28-H28B···O1*, symmetry code*: -1+x, y,1+z, blue dashed line). The molecules in part Λ have been omitted for the sake of clarity.

Needle-shaped crystal of **4** (Figure 5) crystallize in the orthorhombic P*bca* space group with the expected formula of [Fe($H_2B(pz)_2$)(***i*-PrObpydc**)]. The central skeleton is isomorphous to **1**, thus revealing a mononuclear complex (Figure **2**). The crystal structure was determined at both 297 and 90 K to study the reorganization of the coordination geometry expected in the case of a HS ↔ LS transition. The mean value of the Fe-N variation is found to be 0.194 Å, which lies within the expected range for S = 2 ↔ S = 0 transitions in $Fe^{II}N_6$ SCO systems.[10, 13a, 22] A detailed structure analysis reveal that a larger decrease is observed compared to for Fe-N_{py} distances (0.25 Å) as compared to Fe-N_{pz} distances (0.17 Å) after a spin transition which may be mainly accounted for by the fact that such bipy-type ligand acts as a better π-electron acceptor than pyrazolyl ligands.[10] Short interligand contacts involve two types of CH···O interactions, C11-H11···O43* and C35-H35···O37# (symmetry code: *, 1.5-x, 0.5+y, z; #, -1.5+x, 0.5-y, 1-z; Table S4) (Figure 6, top and Figure S5) that give rise to a 2D supramolecular framework (Figure 6, bottom).

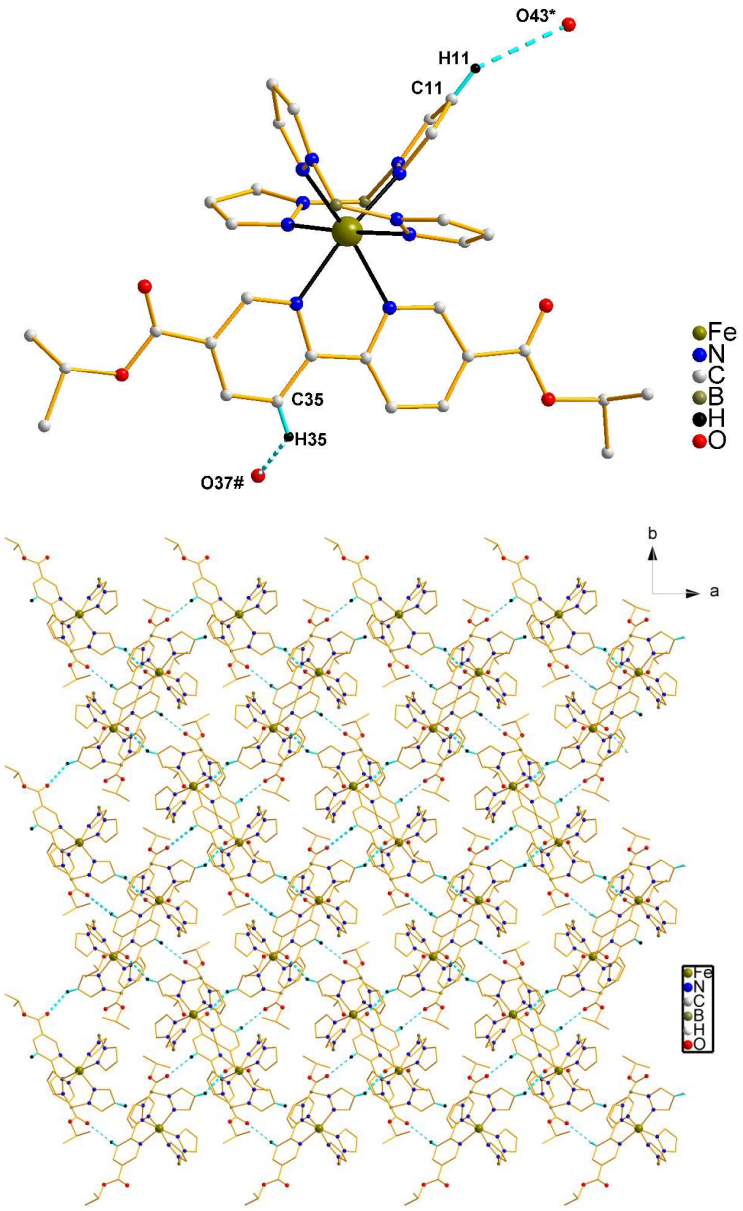

Figure 6. Packing diagram of **4** showing: (top) two types of intermolecular C-H···O interactions (C11-H11···O43* and C35-H35···O37$^{\#}$ (symmetry code: *, 1.5-x, 0.5+y, z; $^{\#}$, -1.5+x, 0.5-y, 1-z; blue dashed line); (bottom) 2D supramolecular framework.

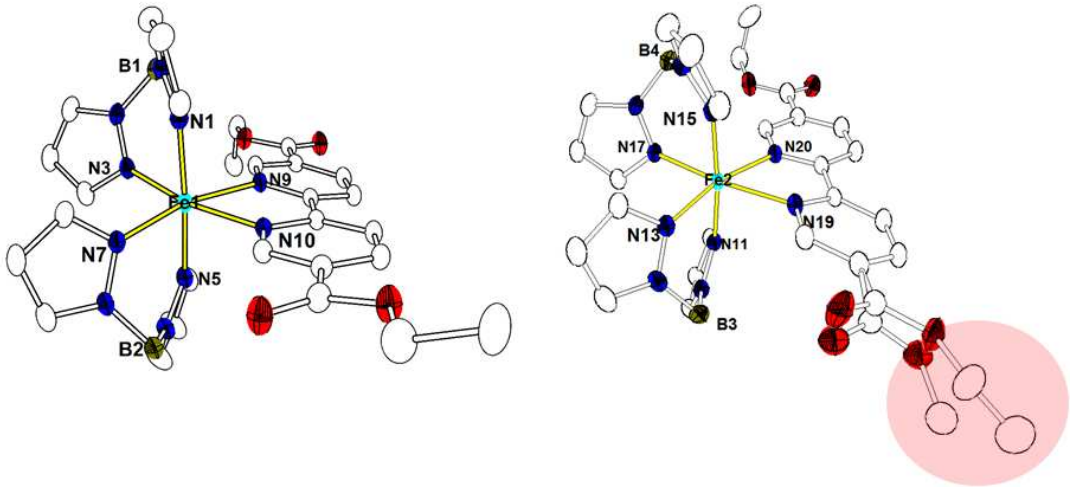

Figure 7 Crystal structure of **3B** at 150 K. Displacement ellipsoids are drawn at the 30% probability level and the H atoms have been omitted for the sake of clarity. The red circle shows the terminal ethyl acetate group in a disordered state with an occupancy factor of 21% whereas an unexpected methyl acetate group is detected with an occupancy factor of 79%.

Unexpected crystal structures of 3B and 4B. Increasing crystallization time afforded translucent dark green prism crystals which were formed after one week. The crystal structure determination revealed however for both complexes, denoted **3B** and **4B**, respectively, an unexpected ligand impurity, as shown in Figures 7 and 9, which will be discussed below.

Complex **3B** crystallizes in the monoclinic space group $P2_1/c$ with two crystallographically independent sites denoted Fe1 and Fe2 (Figure 7). The Fe1 site is composed of one bidentate ligand **EtObpydc** and two $(H_2Bpz_2)^-$ anions, leading to a FeN_6 coordination sphere, similar to the one found in **1**. The situation is dramatically different for the Fe2 site which reveals one terminal ethyl acetate group in a disordered state with an occupancy factor of 21% whereas an unexpected methyl acetate group is detected with an occupancy factor of 79% (Figure 7). It is worth noting that the disorder of the terminal acetate group has significant effect on the Fe^{II} environment, especially on Fe-N_{py} bond length when considering its temperature dependence which was recorded down to 100 K. Indeed, the average Fe-N_{py} bond length for the Fe1 molecule (~2.194 Å) was found to be slightly shorter than that of Fe2 molecule (~2.243 Å) at 100 K. Also, the Fe-N_{py} bond length in the Fe1 molecule is found to decrease with temperature contrary to the Fe2 molecule

(Figure 8). This behavior call for a partial thermally induced SCO for one iron(II) site, which should lead to an incomplete SCO, a result will be confirmed by magnetic measurements (*vide infra*).

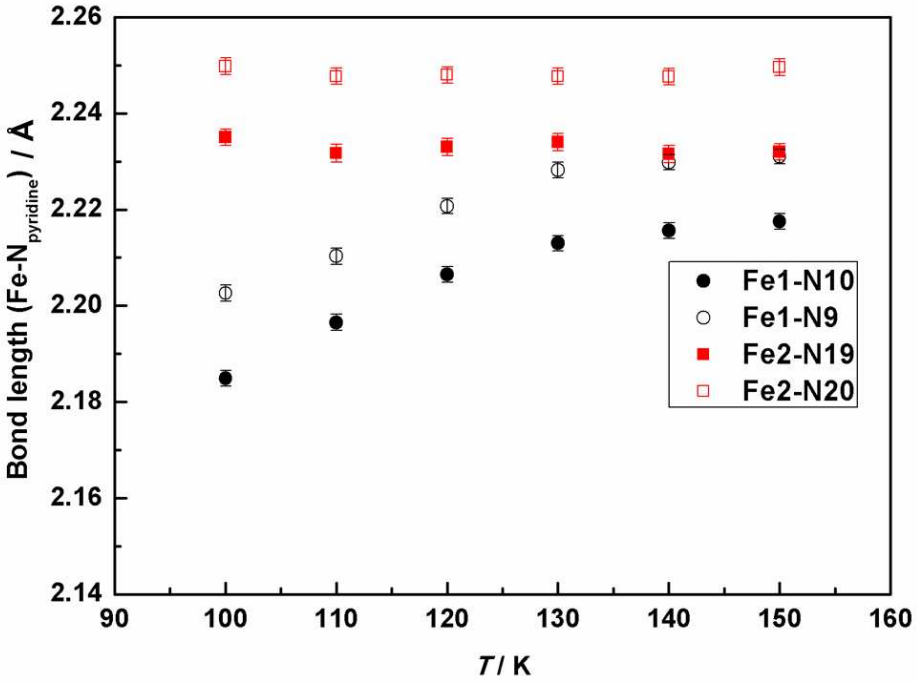

Figure 8. The Fe-N_{py} bond lengths *vs.* temperature for **3B** considering Fe1 and Fe2 sites. Whereas no dependence is detected for the Fe2 site, a smooth decrease in the bond lengths is found for the Fe1 site.

The crystal structure of **4B** was solved at 175 K in the monoclinic space group $P2_1/c$. Two crystallographically independent units, Fe1 and Fe2, are identified (Figure 9). Both Fe1 and Fe2 molecules consist of an Fe atom surrounded by one bidentate **bipy**-typed ligand and two $(H_2Bpz_2)^-$ anions with a Fe–N bond distance of 2.139(2)-2.251(2) Å, indicative of a HS Fe^{II} state (Figure 9).

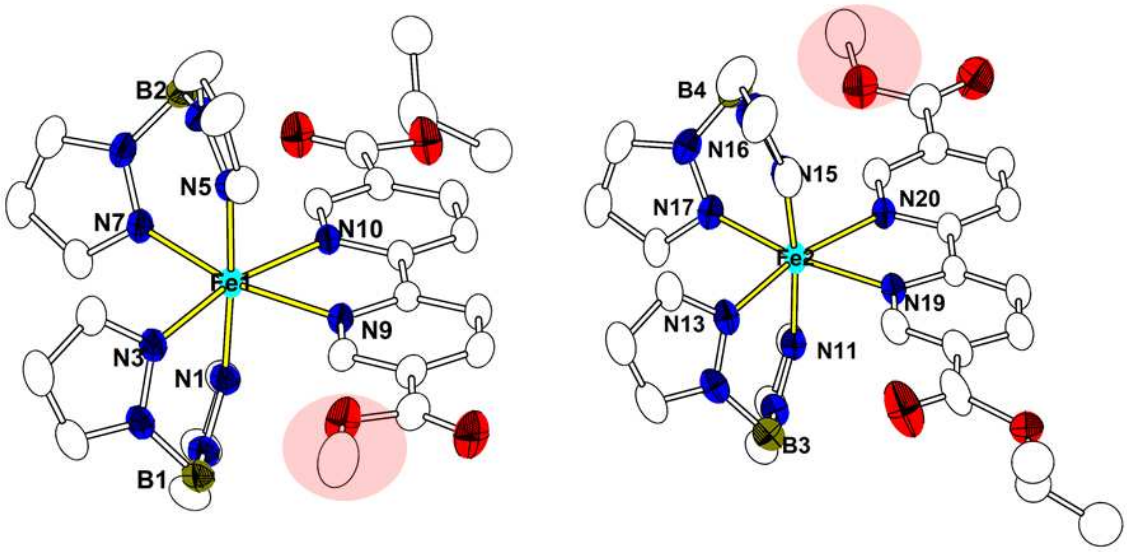

Figure 9. Crystal structure of **4B** at 175 K. Displacement ellipsoids are drawn at the 30% probability level and H atoms have been omitted for the sake of clarity. The red circle shows the unexpected methyl acetate group.

To our surprise, a closer look at the FeN_6 environment reveals that the original ***i*-PrObpydc** ligand has been completely changed into a new asymmetrical ligand L´, where L´ is 5-isopropyl 5'-methyl-2,2'-bipyridine-5,5'-dicarboxylate (Scheme 3). Since the **EtObpydc** and ***i*-PrObpydc** ligands used for the synthesis of **3** and **4**, were free of any impurities, we thought that a transesterification[23], could occur during the crystallization process. This reaction would be catalyzed by a Fe^{III} impurity provided by the Fe^{II} salt used during the synthesis, which would be partially oxidized into Fe^{III}. This impurity would be favored in case a slight excess of $Fe(ClO_4)_2$ would be present in the reaction medium so that the residual of Fe^{III} would run as a catalyst to induce the transesterification from the original iso-propyl group into a methyl group via the MeOH solvent. This process would be more probable in case of a slow reaction, such as a crystallization by slow evaporation.

Scheme 3. Suggested formation mechanism for **4B**

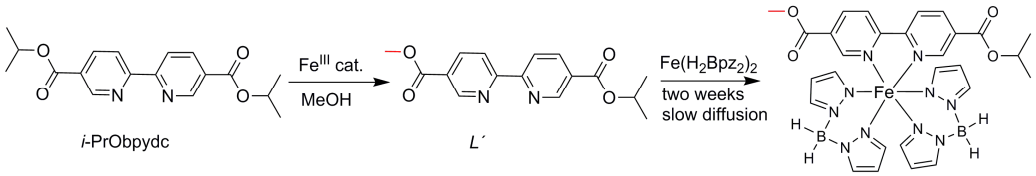

2.3. Spectroscopic and magnetochemical studies

UV−vis diffuse reflectance spectroscopy (DRS). In the solid state, all the powder samples **1**-**4** are strongly thermochromic. At room temperature, complex **1** is pink while other three complexes are green. On cooling, the color changes to deep red for **1** and deep green for **2**, **3** and **4**. For instance, **4** exhibits reversible pronounced thermochromism from green to dark green on quenching of the sample in liquid nitrogen for several seconds (Figure 10). The visible change in color is due essentially to a shift of the charge-transfer transition to lower energy at low temperature.

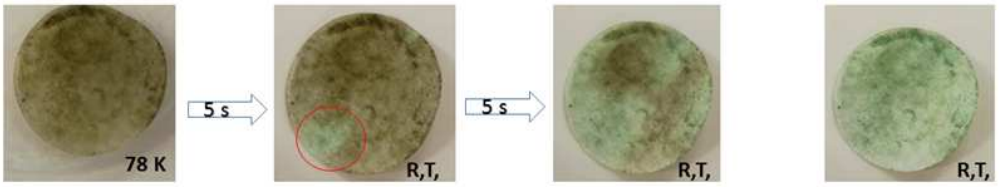

Figure 10. Illustration of thermochromism of powder sample **4** after quench cooling the sample to liquid nitrogen from dark green to green within several seconds.

As observed in Figure 11, a broad-band centred at ~11800 cm^{-1} for **1** can be assigned to a metal-to-ligand charge transfer (MLCT) adsorption from the metal d_{π}-orbitals into π*-orbitals of the ligands.[7, 24] For the other three complexes, such ligand field absorption is shifted to higher energy and further split into the principal component occurring around 14000 cm^{-1} with a shoulder at 12000 cm^{-1}. The splitting arises presumably from Jahn-Teller and/or low symmetry effects associated to the $^5T_{2g} \rightarrow {}^5E_g$ transition.[7] Additionally, the position of the MLCT band changes from the methyl group to the alky acetate series. This indicates that the introduction of an electron-withdrawing alky acetate group leads to an increase in the π-accepting ability of the ligand **bipy**-type,[16] thus influencing the SCO behaviour.

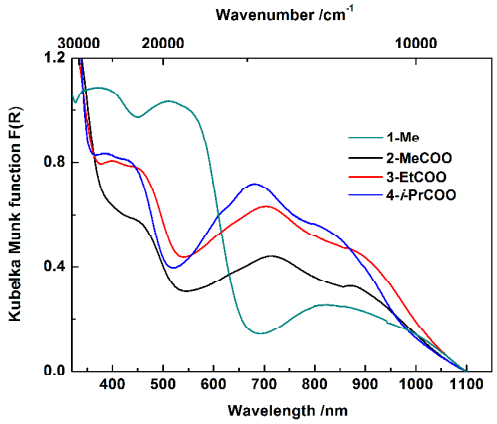

Figure 11. UV−vis DRS of powdered samples **1-4** recorded at room temperature.

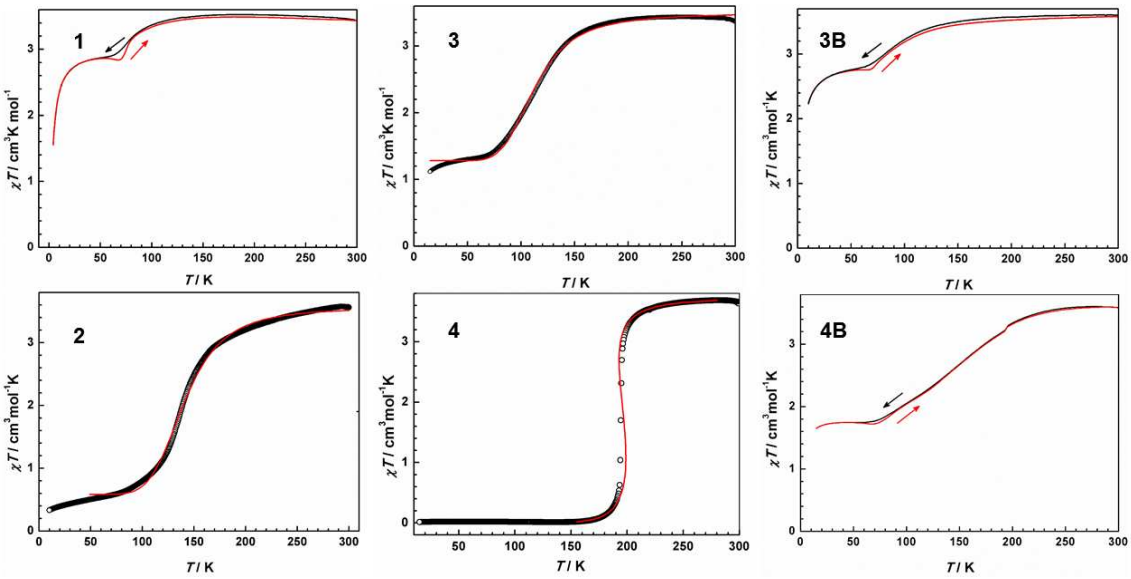

Figure 12. Temperature-dependent $\chi_M T$ plot for all the complexes. The red line for **1**, **3B** and **4B** shows the heating mode. The red solid curve corresponds to data fitting using the ideal solution model[25] for **2** and **3** and Slichter and Drickamer model[26] for **4**.

Magnetic properties. The solid-state magnetic behavior of all the complexes was probed by variable-temperature direct current (dc) susceptibility measurements on polycrystalline samples under an applied field of 1 T. The room temperature $\chi_M T$ values of all complexes except **2** and **4B** ranging around 3.5 cm^3 K mol^{-1} are consistent with pure non-interacting HS Fe^{II} species. Upon cooling, however, different thermal evolutions are recorded as shown in Figure 12.

Complex **1** shows rather unusual magnetic properties. Upon cooling, no dramatic variation is observed down to ca. 150 K, after which a decrease is noticed to drop around 77 K to reach a plateau below 55 K. The sharper decrease observed below 25 K is likely due to zero-field splitting of a large fraction of HS Fe^{II} ions. On warming, no hysteresis loop is detected but a small decrease of the $\chi_M T$ product on warming is noticed, just before the transition temperature of 77K. This behaviour presumably calls for a freezing-in effect[27], that hinders further the spin conversion. ^{57}Fe Mössbauer spectroscopy (*vide infra*), carried out on the same sample batch, confirms the incomplete character of the SCO behaviour with ca. 9.5% of LS Fe^{II} ions being detected at 78 K. The magnetic properties of **3B** resemble the one of **1** with a gradual type transition involving a few spin carriers. Mössbauer spectroscopy informs that 83.3 % of HS Fe^{II} ions are populated at 78 K (vide infra).

Complex **2** undergoes a gradual and almost complete SCO behavior. Indeed, the thermal evolution of $\chi_M T$ continuously decreases from ambient temperature to 170 K, from which it drops to 0.59 $cm^3 K mol^{-1}$ at 80 K, reaching 0.33 $cm^3 K mol^{-1}$ at 10 K. The SCO profile can be fitted well using the ideal solution model[25], leading to $T_{1/2}$ = 140.4(2) K, enthalpy ΔH_{HL} = 8.18(9) kJ mol^{-1} and entropy ΔS_{HL} = 58.4(5) J $K^{-1}mol^{-1}$.

For **3**, the $\chi_M T$ value keeps a nearly constant evolution at 3.36 $cm^3 K mol^{-1}$ in the temperature range 300−210 K, after which it decreases gradually, disclosing a HS → LS conversion with $T_{1/2}$ = 113 K, and reaching a second plateau at 1.28 $cm^3 K mol^{-1}$ over the range 20−60 K, indicative a nearly half-spin transition. No change was observed while recording again the magnetic properties over the range 20−300 K. Fitting the magnetic data using the ideal solution model[25], provides the following thermodynamic parameters associated to the SCO: ΔH_{HL} = 5.90(6) kJ mol^{-1}, ΔS_{HL} = 52.2(4) J $K^{-1}mol^{-1}$ as well as $T_{1/2}$ = 113.4(2) K.

For **4**, the $\chi_M T$ value slowly decreases from 3.60 $cm^3 K mol^{-1}$ at 300 K to 3.04 $cm^3 K mol^{-1}$ at 200 K and then drops steeply at $T_{1/2}$ = 194 K to reach to 0.01 $cm^3 K mol^{-1}$ at 15 K. Such behavior indicates an abrupt spin transition from a HS state (S = 2) at high temperature to a LS ground state (S = 0) at lower temperature. Fitting the magnetic data using the Slitcher and Drickamer model[26] provides the following thermodynamic parameters: ΔH_{HL} = 12.5(1) kJ mol^{-1}, ΔS_{HL} = 63.6(4) J $K^{-1}mol^{-1}$, Γ = 4.16(4) kJ mol^{-1} and $T_{1/2}$ = 195.9(1) K. Such later value nicely corresponds to the recorded transition temperature.

The temperature dependence of the magnetic properties of **4B** resembles the one of **3** with a gradual spin crossover profile which plateau at 1.73 $cm^3 K mol^{-1}$ over the range 20−60 K. Mössbauer spectroscopy informs that ca. 48 % of HS Fe^{II} ions are populated at 78 K (vide infra). Thus, a gradual half-spin conversion was described. Noteworthy is that a knot was detected at 195 K which exactly corresponds to $T_{1/2}$ observed in **4** (Figure S6). This feature suggests that the transesterification is not complete with a residual amount of **4** upon increasing crystallization time to one week.

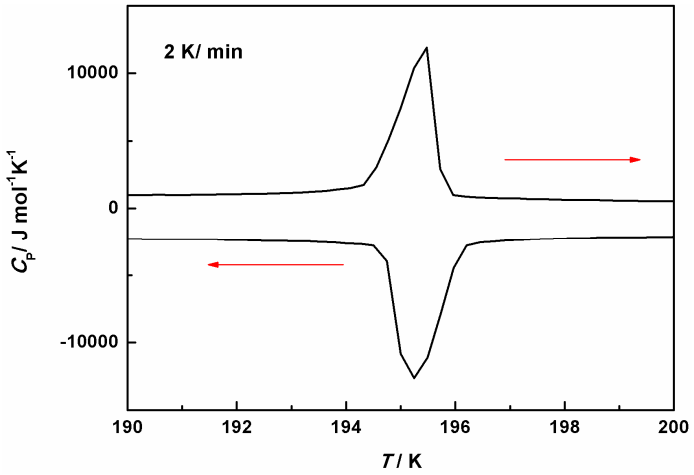

Figure 13. Heat capacity thermal profile on cooling and warming modes of **4** recorded at a scan rate of 2 K/min.

Differential Scanning Calorimetry (DSC). Given the sharp spin transition identified for **4**, this complex was also investigated by differential scanning calorimetry (DSC) on both warming and cooling modes at a 2 K min^{-1} scan rate. Corresponding heat capacity temperature profiles, C_p, are displayed in Figure 13. One exothermic peak, characteristic of a first order phase transition, is identified on cooling at $T_{max}^{\downarrow}$ = 195.5 K. On warming, an endothermic peak is observed at $T_{max}^{\uparrow}$ = 195.5 K, thus delineating no hysteresis effect. The variations of enthalpy (ΔH_{HL}) and entropy (ΔS_{HL}) have been determined as ΔH_{HL} = 11.9 kJ mol^{-1} and ΔS_{HL} = 60.7 J K^{-1}mol^{-1}. These values are within the experimental range for Fe^{II} SCO systems[28]. The entropy gain is found to be much larger than the electronic contribution to the entropy, R·ln(5) = 13.4 J K^{-1}mol^{-1}, for Fe^{II} SCO complexes.[29] This is due to a high extent to the vibrational entropy which was identified as 47.3 J K^{-1}mol^{-1}.

Table 1 ^{57}Fe Mössbauer parameters for all the complexes

Complex	T/ K	A_{HS}/A_{tot}(%)	HS Fe^{II} (mm/s)			Fe^{II} LS (mm/s)			Fe^{III} (mm/s)		
			δ	ΔE_Q	Γ/2	δ	ΔE_Q	Γ/2	δ	ΔE_Q	Γ/2
1[a]	298	100	1.01(4)	1.84(8)	0.15(6)						
	78	90.5(3)	1.12(4)	2.53(8)	0.15(8)	0.50(1)	0.33(2)	0.23(2)			
2[b]	298	88.3(5)	1.01(1)	2.41(3)	0.25(3)	0.49(2)	0.71(1)	0.19(1)			
	78	21(2)	1.12(1)	3.11(3)	0.20(3)	0.48(3)	0.65(5)	0.17(6)			
3[a]	298	100	1.01(3)	2.00(5)	0.23(4)						
	78	46.9(2)	1.12(6)	2.76(1)	0.16(9)	0.50(5)	0.55(9)	0.16(7)			
4[a]	298	100	0.99(5)	1.80(1)	0.16(8)						
	78	0				0.48(3)	0.66(5)	0.16(3)			
3B[a]	298	100	1.02(8)	1.99(2)	0.23(1)						
	78	83.3(1)	1.12(2)	2.68(4)	0.17(3)	0.50(1)	0.57(2)	0.16(2)			
4B[a]	298	63.4(5)	1.00(1)	2.21(3)	0.19(2)				0.33(4)	0.65(7)	0.26(5)
	78	47.8(6)	1.12(3)	2.64(7)	0.30(5)	0.49(2)	0.71(3)	0.23(2)			

δ: isomer shift (with respect to α-Fe at 298 K); ΔE_Q: quadrupole splitting: $\Gamma/2$: half width at half maximum. a: grounded crystals; b: powder sample.

^{57}Fe Mössbauer spectroscopy. Temperature-dependent zero-field ^{57}Fe Mössbauer spectroscopy was applied to investigate the stability of our materials (oxidation of iron) and to determine the nature of spin states at low and high temperatures (Figures 14 and S7). As shown in Table 1, all the complexes display an isomer shift (δ) of ~ 1 mm s^{-1} at room temperature. An identical room temperature isomer shift was found for the mononuclear SCO complex [$Fe(H_2B(pz)_2)_2$phen*], where phen* is a diarylethene-derived phenanthroline ligand[13a]. The listed Mössbauer parameters point unambiguously to the presence of HS $Fe^{II}N_6$ species at room temperature. For **2**, LS Fe(II) ions with an isomer shift (δ) of 0.49 mm s^{-1} are in addition identified whereas for **4B**, Fe(III) species reflected by an isomer shift (δ) of 0.33 mm s^{-1} are revealed at room temperature (Figure S7). Upon cooling to 78 K, the isomer shift increases to δ = 1.12 mm s^{-1} due to the expected second-order Doppler shift[30], and the quadrupole splitting ΔE_Q becomes as large as 3.11 mm s^{-1} for **2**. More importantly, a new quadrupole doublet appears for all the complexes with a relative intensity of a full population for **4**, which is characterized by a lower isomer shift around 0.50 mm s^{-1} and a much smaller quadrupole splitting ΔE_Q < 1.0 mm s^{-1}. This later signal is characteristic for a LS Fe^{II} ion in a distorted pseudooctahedral environment. Incomplete SCO behavior is thus identified for **1**, **2**, **3, 3B** and **4B** contrary to **4**.

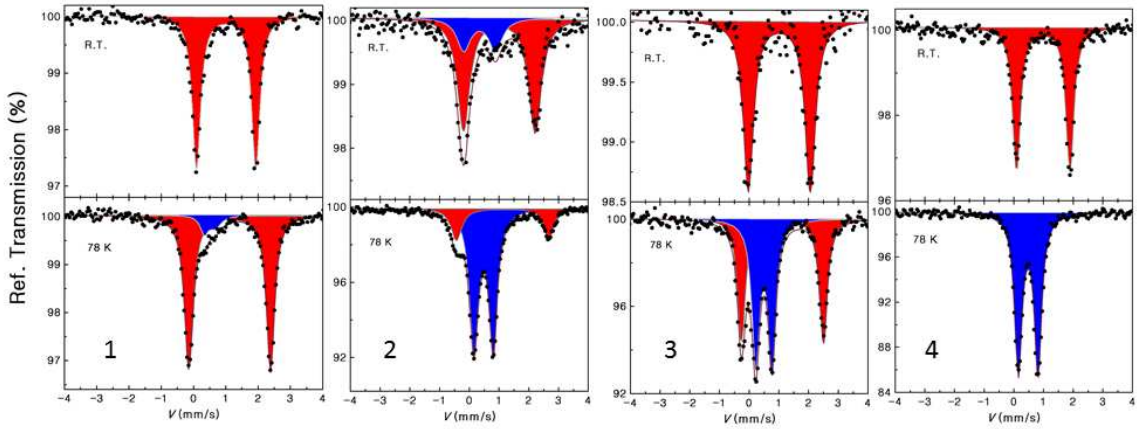

Figure 14 ^{57}Fe Mössbauer spectra of polycrystalline samples for all the complexes recorded at 298 K (top) and 78 K (bottom). Red and blue correspond to the Fe^{II} HS and LS doublets, respectively.

DFT calculations. In order to probe the influence of electronic substituents on SCO,

we carried out density functional calculations for complexes **1**-**4** using the ORCA 4.0.0. program[31]. Geometry optimizations were started from the single crystal X-ray structure data using the BP86 functional in combination with the def2-SVP basis set on all atoms with the exception of Fe, for which the triple-ζ def2-TZVP basis set was used. The HS state for **1** can be attributed to the relatively small energy difference (Δ) between the highest d_{π}-orbital and the d_{z^2}-orbital, while the series **2** to **4** bearing different ester group turned out to reveal a relatively large energy splitting of Δ and stronger π-acceptor properties, which stabilized the LS state[16] (Figures S8-S12). Within the series **2** to **4**, however, the difference between the ligand field strengths of the various acetate ligands is negligible (Figure S8), which indicates that the crystal packing plays an important role in switching the SCO[14] (*vide infra*).

3. DISCUSSION

In our system, the SCO behavior is drastically different from complexes to complexes caused by subtle but crucial structural differences between the respective $Fe^{II}N_6$ skeleton. It is well known that the prototype of $[Fe(H_2Bpz_2)_2(bipy)]$ complex (**5**) has been reported to show thermally induced spin transition[10]. However, the introduction of different aromatic directing groups into the bipy ligand can affect the π-acceptor character, leading to the distinction of ligand field strength and diversity of SCO properties.[16] As a typical electron withdrawing groups, ester moieties in **2**, **3** and **4** are good candidates to support the bipy ligands acting as a better π-electron acceptor. This point has been reflected by the shorter Fe-N_{py} distances (1.968(1) and 1.964(1) Å) observed for **4** in the LS state compared to **5** (2.013(2) Å). The BP86 calculations for the discussed complexes also revealed that the energy difference (Δ) between the highest d_{π}-orbital and the d_{z^2}-orbital of 2.70 eV for **2**, **3** and **4** is slightly larger than that of 2.67 eV for **1** (Figure S8). Therefore, the introduction of electron-withdrawing substituents leads to strengthened ligand field strength of those ester series. On the other hand, crystal-packing effect has been shown to influence the magnetic properties of Fe^{II} SCO complexes, illustrating explicitly the importance of the crystalline arrangement for realizing special cooperative behavior. Closer inspection between **3** and **4** crystal structures reveals main differences which can be summarized as follows:

(a) **Supramolecular interactions**: both crystal packing of **3** and **4** are dominated by C-H···O interactions but with different supramolecular structures (Figures 5 and 6).

3 displays a C_{sp}^3-H···O interaction between carbonyl oxygen and ethyl β carbon atom, which is located far away from iron(II) centers. **4**, in turn, undergoes two kinds of C-H···O interactions forming a 2D supramolecular structure. More importantly, both two types of proton donor in **4** originate from py and pz rings, which are directly coordinated to the Fe^{II} ion. Therefore, these C-H···O interactions, as a catalog of weak H-bonds,[32] can shifts in electron density that accompany the magnitudes of the various components of the interaction energy to influence cooperative SCO behavior.

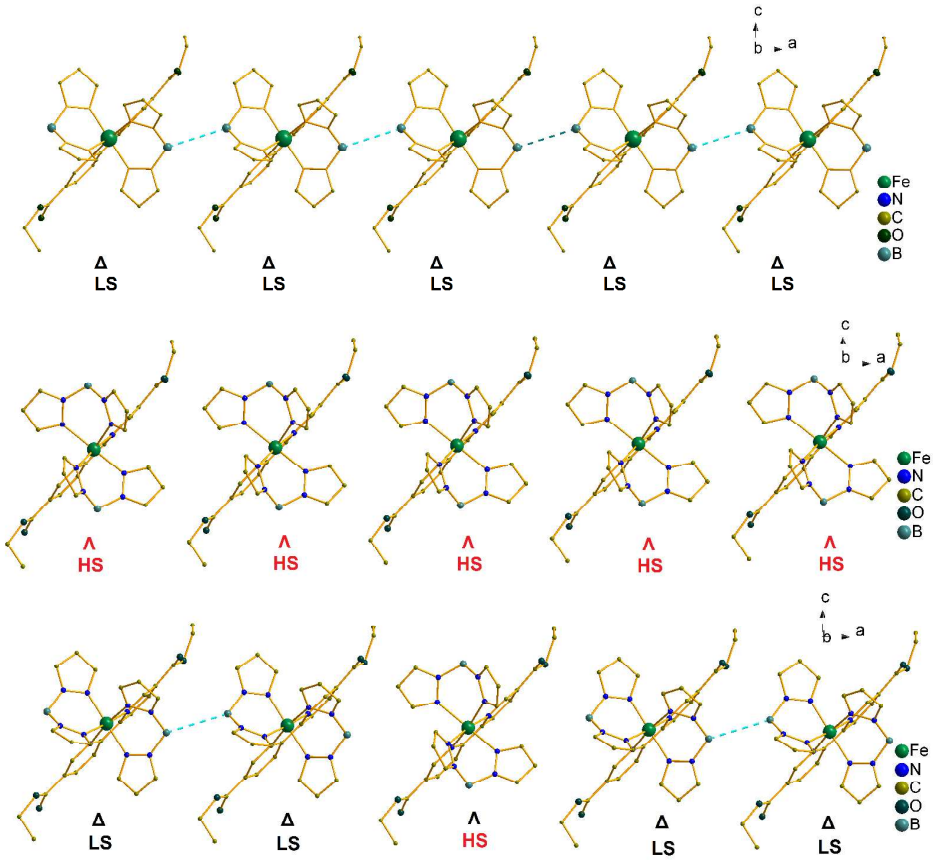

Figure 15. Illustration of the crystal packing for the Δ isomer with the ordered H_2Bpz_2 ligands (top), Λ isomer with the ordered H_2Bpz_2 ligands (middle) and with the disordered H_2Bpz_2 ligands in **3** (bottom).

(b) **Structural disorder**: it is the disordered H_2Bpz_2 ligands in **3** which clearly affect the SCO properties between two different enantiomers. As shown in Figure 15, in ordered Δ isomers, there is a B···B short contact from the adjacent H_2Bpz_2 ligands at a distance of 3.626 Å. This B···B contact was strongly contracted as short as 3.475 Å at 92K and even to 3.452 Å at 20K. Such contraction is observed for the first time for $[Fe(H_2Bpz_2)_2(L)]$ related complexes. In addition, to the best of our knowledge, this

distance is the shortest B···B contact so far found for a 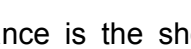 stacking motif, based on a CCDC search (Figure S13). The B···B distances at low temperatures were much shorter than the Van der Waals radii of B---B contact (3.6-4.1 Å)[33], indicating a crowded stacking for the Δ configuration to a certain extent (Figure 15, top). However, this crowded situation can be avoided by changing the Δ configuration to the Λ one as shown in Figure 15, middle. Therefore, the disorder in **3** can be viewed as the insertion of Λ molecules into the ordered Δ lattices, breaking down the boron contact of H_2Bpz_2 chain to a short range one (Figure 15, bottom). The LS molecules are conducted within these "crowded" short chains, while the HS molecules are kept in these disordered Λ species, because of their "roomy" surroundings. Fe^{II} compounds showing incomplete or intermediate SCO have been reported[34], based on the hypothesis that SCO sites are strongly depends on cooperativity (hydrogen bonds, π–π stacking, and van der Waals interactions within the crystal lattice), leading to a specific stoichiometric combination of HS and LS Fe^{II} molecules. The cooperativity in disordered structure of **3** presented here, demonstrates that the control of chiral enantiomers within crystal packing can become an outlet for development of new molecular devices based on SCO materials

4. CONCLUSION

The foregoing results demonstrate that subtle, remote variation of the ligand field can lead to significant modulation of the transition temperature in $[Fe(H_2Bpz_2)_2(bipy\text{-}type)]$ SCO complexes with electronic substituent-decorated 5,5´-positioned bipy ligands. Importantly, the electronic substituent effect isopropyl acetate group and C-H···O supramolecular interactions in **4** contribute to efficient elastic interactions associated to the spin crossover behavior, leading to an abrupt thermally induced spin transition. This example thus pinpoints the importance of supramolecular interactions, to design highly cooperative SCO complexes,[35] which is of key relevance for mononuclear complexes where no important cooperative effects are expected.[36] The addition of electronegative atoms on the bipy ligands increase the low-lying π-acceptor characters, which are suitably oriented for interaction with the filled d_π orbitals of the metal atom and therefore for strengthening the metal–ligand interaction. Further in-depth studies including theoretical calculation on this system are required to

elucidate the underlying mechanism. This methodology, which can provide a tool for the further design and fabrication of SCO materials switching at higher temperature, is currently under consideration in our laboratory. In addition, their higher thermal stability is an important assess for these materials in view of their future nanostructuration as thin films, e.g. using CVD processes.

5. EXPERIMENTAL SECTION

Syntheses. All chemicals were used as commercially obtained without further purification.

Synthesis of bipyridine derivatives. 2,2′-Bipyridine-5,5′-dicarboxylic acid (**bpydc**)[17], dimethyl-2,2'-bipyridyl-5,5'-dicarboxylate (**MeObpydc**)[18], diethyl-2,2'-bipyridyl-5,5'-dicarboxylate (**EtObpydc**)[19] and diisopropyl-2,2'-bipyridine-5,5'-dicarboxylate (***i*-PrObpydc**)[20] were prepared using literature procedures.

Synthesis of complexes 1-4: Syntheses were performed under $Ar_{(g)}$ using Schlenk techniques.

[$Fe(H_2Bpz_2)_2$(**bipy-CH_3**)] (**1**). To a solution of $K[H_2B(pz)_2]$ (160 mg, 0.88 mmol) in methanol (5 mL) was added a solution of $Fe(ClO_4)_2 \cdot 6H_2O$ (160 mg, 0.44 mmol) in methanol (5 mL). The formed $KClO_4$ precipitate was removed by filtration, affording a yellow solution. A solution of **bipy-CH_3** (81 mg, 0.44 mmol) in methanol (10 mL) was then added dropwise to the solution, causing an immediate color change to dark pink. After the solution was stirred for 2 h at room temperature, a pink precipitate was collected, washed with methanol, and dried under a stream of $N_{2(g)}$. Yield: 158 mg (67%). Anal. Calcd. for **1** ($C_{24}H_{28}N_{10}B_2Fe$): C, 53.98; H, 5.28; N, 26.23. Found: C, 53.06; H, 5.15; N, 26.33. MS (FTMS+pESI): m/z: 535.21 [M^+]. Single crystals of **1** were obtained by slow diffusion in methanol under $Ar_{(g)}$, using a single-tube glass vessel. The **bipy-CH_3** in CH_3OH was placed on the top of a $Fe(H_2B(pz)_2)_2$ methanolic solution. Pink-violet single crystals of [$Fe(H_2Bpz_2)_2$(**bipy-CH_3**)] (**1**), suitable for X-ray diffraction analysis, formed after one week.

[$Fe(H_2Bpz_2)_2$(**MeObpydc**)] (**2**). The same method as for **1** was followed using **MeObpydc** (120 mg, 0.44 mmol), which yielded to an olive-green precipitate of **2**. Yield: 165 mg (60%). Anal. Calcd for **2** ($C_{26}H_{28}N_{10}B_2O_4Fe$): C, 50.20; H, 4.54; N, 22.52. Found: C, 51.73; H, 4.53; N, 20.71. MS (FTMS+pESI): m/z: 623.19 [M^+]. Attempts to crystallize complex **2** failed due to the poor solubility of **MeObpydc**.

[$Fe(H_2Bpz_2)_2$(**EtObpydc**)] (**3**). The same method as for **1** was followed using **EtObpydc** (130 mg, 0.44 mmol), which yielded to an olive-green precipitate. Yield: 166 mg (56%). Anal. Calcd for **3** ($C_{28}H_{32}N_{10}B_2O_4Fe$): C, 51.73; H, 4.96; N, 21.55. Found: C, 50.99; H, 4.75; N, 21.83. MS (FTMS+pESI): m/z: 651.22 [M^+]. Single crystals were obtained by slow diffusion in methanol/dichloromethane mixture under Ar using a single-tube glass vessel. The **EtObpydc** in CH_2Cl_2 was placed on the bottom of $Fe(H_2B(pz)_2)_2$-containing methanol solution, affording green needle crystals, namely **3**, suitable for X-ray diffraction analysis, after overnight. Increasing crystallization time up to one week afforded prism shape crystals, which were identified as **3B**.

[$Fe(H_2Bpz_2)_2$(***i*-PrObpydc**)] (**4**). The same method as for **1** was followed using ***i*-PrObpydc** (140 mg, 0.44 mmol), which yielded to an olive-green precipitate. Yield: 168 mg (54%). Anal. Calcd. for **4** ($C_{30}H_{36}N_{10}B_2O_4Fe$): C, 53.13; H, 5.35; N, 20.65.

Found: C, 51.96; H, 5.27; N, 20.48. MS (FTMS+pESI): m/z: 679.25 [M^+]. The same crystallization method was followed as for **3** to afford single crystals of **4** using ***i*-PrObpydc** instead of **EtObpydc**. Increasing crystallization time up to one week afforded crystals of another morphology, namely **4B**.

Characterization Techniques. Elemental analysis for C, H, and N were performed at Medac. NMR spectra were recorded at room temperature. with a Bruker Avance II 300 MHz instrument. Chemical shifts (δ) are reported in ppm from $CDCl_3$ (δ = 7.27 ppm) or DMSO-d^6 (δ = 2.50 ppm) for ^{1}H NMR. Mass spectra (MS) were recorded using Q-Exactive from ThermoFisher spectrometer. Infrared spectra were recorded on Shimadzu FTIR-8400S with KBr pellets. Diffuse reflectance spectra (DRS) were obtained with a PerkinElmer Lambda 9 UV/Vis/NIR spectrophotometer equipped with a 60 mm integrating sphere and converted into absorption spectra by using the Kubelka–Munk function, using $BaSO_4$ as a reference. Thermogravimetric analyses (TGA) were performed in $N_{2(g)}$ (100 mL min^{-1}) at a heating rate of 10 $Kmin^{-1}$ from 298 to 873 K using a Mettler Toledo TGA/SDTA 851e analyser. Magnetic susceptibilities were measured on a Quantum design MPMS-5s SQUID magnetometer. The magnetic data were corrected for the sample holder and diamagnetic contributions. The crystal sample was quickly loaded into a gelatin capsule and immediately inserted within the SQUID cavity. ^{57}Fe Mössbauer spectra were recorded in transmission geometry with a constant acceleration mode conventional spectrometer equipped with a 50 mCi ^{57}Co(Rh) source and a Reuter Stokes proportional counter. The powdered samples were sealed in aluminum foil and spectra were recorded at 298 and 78 K. All samples were grounded because spectra of fresh crystals systematically afforded line dissymmetry due to texture. The spectra were fitted using Recoil 1.05 Mössbauer Analysis software[37]. The isomer shift values are given with respect to α-Fe at 298 K.

Single Crystal X-ray Analyses. Suitable single crystals were selected for single-crystal X-ray diffraction analysis. 20 K data for complexes **1** and **3** were collected with an Oxford Diffraction Xcalibur3 diffractometer, using monochromated Mo-Kα radiation (λ = 0.71073 Å). The diffractometer was fitted with a liquid helium low-temperature device, Helijet Oxford Diffraction Cryostat. Crystallographic data at other temperatures were collected on a MAR345 image plate using MoKα radiation (λ = 0.71073Å). The crystals were selected, mounted in inert oil and transferred to the cold gas stream for flash cooling. Data were integrated by CrysalisAlisPro (Agilent Technologies (2014), Agilent Technologies UK Ltd., Oxford, UK, Xcalibur/SuperNova CCD system, CrysAlisPro Software system, Version 1.171.37.35 and 1.171.38.41). Absorption correction was applied using the integrated multi-scan absorption algorithm. The structures were solved by direct methods (SHELXS) and refined by full-matrix least-squares on F^2 using SHELXL2014[38]. The location of Fe atom was easily determined, and O, N, and C atoms were subsequently located in the difference Fourier maps. The non-hydrogen atoms were refined anisotropically. The H atoms were introduced in calculated positions and refined with fixed geometry with respect to their carrier atoms. DFIX, FLAT, DELU, SAME, ISOR and EADP constrains were applied in the refinement of the disordered boron-containing pyrazoyl group and alkyl ester substituents. CCDC 1829354 (**1**_95 K), 1832091 (**2**_20 K), 1829355 (**3**_296 K), 1829358 (**3**_92 K), 1832092 (**3**_20 K), 1829356 (**4**_297 K), 1829357 (**4**_90 K), 1832660 (**3B**_150 K), 1829660 (**3B**_100 K) and 1829661 (**4B**_175 K) are the supplementary crystallographic data for this paper. They can be obtained free of charge from the Cambridge Crystallographic Data Center via www.ccdc.cam.ac.uk/data_request/cif.

DFT calculations. All calculations were performed using the ORCA 4.0.0.program[31]. Geometry optimizations were started from the X-ray structure data using the BP86 functional in combination with the def2-SVP basis set on all atoms with the exception of Fe, for which the triple-ζ def2-TZVP basis set was used. These calculations made use of the RI density fitting approximations implemented in ORCA, using def2/J auxiliary basis set[39]. Based on the optimized geometries single-point energy calculations were carried out with the B3LYP functional in conjunction with the def2-TZVP basis set. All calculations employed the relativistic recontracted version of the def2 basis sets[40], the zeroth order relativistic approximation (ZORA)[41] and D3 dispersion correction with Becke-Johnson damping function (D3(BJ))[42]. Second-derivative calculations were carried out for all structures to ensure that they are minima on the potential energy surface. The DFT calculations predicted a very stable LS ground state for all the complexes using BP86 while B3LYP predicted the HS state to lie below the LS state by about 3 kcal/mol[43].

ASSOCIATED CONTENT

Supporting Information

The Supporting Information is available free of charge on the ACS Publications website at DOI: 10.1021/acs.inorgchem.xxxx

Overview of IR, structure and crystallographic data, Magnetic data for **4B**, Mössbauer of **3B** and **4B** as well as computed frontier molecular orbitals for **1**-**4**.

AUTHOR INFORMATION

Corresponding Author

*E-mail: yann.garcia@uclouvain.be.

Notes

The authors declare no competing financial interest.

ACKNOWLEGDEMENT

We acknowledge financial support from FNRS (PDR T.0102.15), Romanian National Authority for Scientific Research, CNCS−UEFISCDI, Project No. PN-II-RU-TE-2014-4-2695, FNRS-Academie Roumaine, WBI Roumanie, and COST Action Nos. CM1305 and CA15128. S. X. (24918505) and Y. GUO (28109061) are chargé de recherches from the FNRS. We thank Prof. J. Wouters for the courtesy use of a diffuse reflectance spectrometer.

REFERENCES

(1) (a) Gütlich, P.; Gaspar, A. B.; Garcia, Y. Spin state switching in iron coordination compounds. *Beilstein J. Org. Chem.* **2013,** *9*, 342-391;(b) Molnár G.; Rat, S.; Salmon, L.; Nicolazzi, W.; Bousseksou, A. Spin Crossover Nanomaterials: From Fundamental Concepts to Devices. A*dv Mater.* **2018**, 30, 1703862.

(2) Zhao, T.; Boldog, I.; Spasojevic, V.; Rotaru, A.; Garcia, Y.; Janiak, C. Solvent-triggered relaxative spin state switching of $[Fe(HB(pz)_3)_2]$ in a closed nano-confinement of NH_2-MIL-101(Al). *J. Mater. Chem. C* **2016,** *4*, 6588-6601.

(3) Murray, K. S.; Kepert, C. J. Cooperativity in spin crossover systems: memory, magnetism and microporosity. *Top. Curr. Chem.* **2004,** *233*, 195-228.

(4) Brooker, S. Spin crossover with thermal hysteresis: practicalities and lessons learnt. *Chem. Soc. Rev.* **2015,** *44*, 2880-2892.
(5) Goodwin, H. A. Spin crossover in iron(II) tris(diimine) and bis(terimine) systems. *Top. Curr. Chem.* **2004,** *233*, 59-90.
(6) Onggo, D.; Goodwin, H. Steric Effects of the Spin State of Iron(II) in Complexes of Substituted Bipyridine Derivatives. *Aust. J. Chem.* **1991,** *44*, 1539-1551.
(7) Onggo, D.; Hook, J. M.; Rae, A. D.; Goodwin, H. A. The influence of steric effects in substituted 2,2′ -bipyridine on the spin state of iron(II) in $[FeN_6]^{2+}$ systems. *Inorg. Chim. Acta* **1990,** *173*, 19-30.
(8) James, B. R.; Parris, M.; Williams, R. J. P. Spectrophotometric and thermodynamic properties of some copper and iron complexes. *J. Chem. Soc.* **1961**, 4630-4637.
(9) Büldt, L. A.; Prescimone, A.; Neuburger, M.; Wenger, O. S. Photoredox Properties of Homoleptic d6 Metal Complexes with the Electron-Rich 4,4′ ,5,5′ -Tetramethoxy-2,2′ -bipyridine Ligand. *Eur. J. Inorg. Chem.* **2015,** *2015*, 4666-4677.
(10) Real, J. A.; Muñoz, M. C.; Faus, J.; Solans, X. Spin Crossover in Novel Dihydrobis(1-pyrazolyl)borate $[H_2B(pz)_2]$-Containing Iron(II) Complexes. Synthesis, X-ray Structure, and Magnetic Properties of $[FeL\{H_2B(pz)_2\}_2]$ (L = 1,10-Phenanthroline and 2,2'-Bipyridine). *Inorg. Chem.* **1997,** *36*, 3008-3013.
(11) Galet, A.; Gaspar, A. B.; Agusti, G.; Muñoz, M. C.; Levchenko, G.; Real, J. A. Pressure Effect Investigations on the Spin Crossover Systems $\{Fe[H_2B(pz)_2]_2(bipy)\}$ and $\{Fe[H_2B(pz)_2]_2(phen)\}$. *Eur. J. Inorg. Chem.* **2006,** *2006*, 3571-3573.
(12) Moliner, N.; Salmon, L.; Capes, L.; Muñoz, M. C.; Létard, J.-F.; Bousseksou, A.; Tuchagues, J.-P.; McGarvey, J. J.; Dennis, A. C.; Castro, M.; Burriel, R.; Real, J. A. Thermal and Optical Switching of Molecular Spin States in the $\{[FeL[H_2B(pz)_2]_2\}$ Spin-Crossover System (L = bpy, phen). *J. Phys. Chem. B* **2002,** *106*, 4276-4283.
(13) (a) Milek, M.; Heinemann, F. W.; Khusniyarov, M. M. Spin Crossover Meets Diarylethenes: Efficient Photoswitching of Magnetic Properties in Solution at Room Temperature. *Inorg. Chem.* **2013,** *52*, 11585-11592; (b) Rösner, B.; Milek, M.; Witt, A.; Gobaut, B.; Torelli, P.; Fink, R. H.; Khusniyarov, M. M. Reversible Photoswitching of a Spin-Crossover Molecular Complex in the Solid State at Room Temperature. *Angew. Chem., Int. Ed.* **2015,** *54*, 12976-12980; (c) Moertel, M.; Witt, A.; Heinemann, F. W.; Bochmann, S.; Bachmann, J.; Khusniyarov, M. M. Synthesis, Characterization, and Properties of Iron(II) Spin-Crossover Molecular Photoswitches Functioning at Room Temperature. *Inorg. Chem.* **2017,** *56*, 13174-13186.
(14) Kulmaczewski, R.; Shepherd, H. J.; Cespedes, O.; Halcrow, M. A. A Homologous Series of $[Fe(H_2Bpz_2)_2(L)]$ Spin-Crossover Complexes with Annelated Bipyridyl Co-Ligands. *Inorg. Chem.* **2014,** *53*, 9809-9817.
(15) Luo, Y.-H.; Liu, Q.-L.; Yang, L.-J.; Sun, Y.; Wang, J.-W.; You, C.-Q.; Sun, B.-W. Magnetic observation of above room-temperature spin transition in vesicular nano-spheres. *J. Mater. Chem. C* **2016,** *4*, 8061-8069.
(16) Luo, Y.-H.; Nihei, M.; Wen, G.-J.; Sun, B.-W.; Oshio, H. Ambient-Temperature Spin-State Switching Achieved by Protonation of the Amino Group in $[Fe(H_2Bpz_2)_2(bipy\text{-}NH_2)]$. *Inorg. Chem.* **2016,** *55*, 8147-8152.
(17) Venema, F.; Nelissen, H. F. M.; Berthault, P.; Birlirakis, N.; Rowan, A. E.; Feiters, M. C.; Nolte, R. J. M. Synthesis, Conformation, and Binding Properties of Cyclodextrin Homo- and Heterodimers Connected through Their Secondary Sides. *Chem. - Eur. J.* **1998,** *4*, 2237-2250.
(18) Case, F. H. The Synthesis of Certain Substituted 2,2'-Bipyridyls. *J. Am. Chem. Soc.* **1946,** *68*, 2574-2577.
(19) Günyar, A.; Betz, D.; Drees, M.; Herdtweck, E.; Kühn, F. E. Highly soluble dichloro, dibromo and dimethyl dioxomolybdenum(VI)-bipyridine complexes as catalysts for the epoxidation of olefins. *J. Mol. Catal. A: Chem.* **2010,** *331*, 117-124.
(20) Delaive, P. J.; Lee, J. T.; AbruÑA, H.; Sprintschnik, H. W.; Meyer, T. J.; Whitten, D. G., Light-Induced Electron Transfer Reactions of Hydrophobic Analogs of $Ru(bipy)_3^{2+}$. In *Inorganic and Organometallic Photochemistry*, AMERICAN CHEMICAL SOCIETY: 1978; Vol. 168, pp 28-43.
(21) Marchivie, M.; Guionneau, P.; Létard, J. F.; Chasseau, D.; Howard, J. A. K. Thermal trapped iron(II) high spin state investigated by X-ray diffraction. *J. Phys. Chem. Solids* **2004**, *65*, 17-23.

(22) Konig, E.; Ritter, G.; Kulshreshtha, S. K. The nature of spin-state transitions in solid complexes of iron(II) and the interpretation of some associated phenomena. *Chem. Rev.* **1985,** *85*, 219-234.
(23) Kumar, B.; Kumar, H.; Parmar, A. Iron(III) Perchlorate: A Reagent for Transesterification. *Indian J. Chem., Sect. B: Org. Chem. Incl. Med. Chem.* **1993,** *32*, 292-293.
(24) Ferrere, S.; Gregg, B. A. Photosensitization of TiO_2 by $[Fe^{II}(2,2'$-bipyridine-4,4'-dicarboxylic $acid)_2(CN)_2]$: Band Selective Electron Injection from Ultra-Short-Lived Excited States. *J. Am. Chem. Soc.* **1998,** *120*, 843-844.
(25) Gütlich, P.; Garcia, Y.; Spiering, H., Spin transition phenomena. In *Magnetism: Molecules to Materials IV: Nanosized Magnetic Materials*, Joel S. Miller, M. D., Ed. Wiley-VCH Verlag GmbH & Co. KGaA: 2003; pp 271-344.
(26) Slichter, C. P.; Drickamer, H. G. Pressure - Induced Electronic Changes in Compounds of Iron. *J. Chem. Phys.* **1972,** *56*, 2142-2160.
(27) Mishra, V.; Mukherjee, R.; Linares, J.; Codjovi, E.; Varret, F.; Lawson-Daku, M. Spin-transition in nearly cubic site in $[Fe^{II}(L)_3][PF_6]_2$. *Hyperfine Interact.* **2009,** *188*, 71-78.
(28) Gütlich, P.; Garcia, Y.; Goodwin, H. A. Spin crossover phenomena in Fe(II) complexes. *Chem. Soc. Rev.* **2000,** *29*, 419-427.
(29) Dîrtu, M. M.; Naik, A. D.; Rotaru, A.; Spinu, L.; Poelman, D.; Garcia, Y. FeII Spin Transition Materials Including an Amino–Ester 1,2,4-Triazole Derivative, Operating at, below, and above Room Temperature. *Inorg. Chem.* **2016,** *55*, 4278-4295.
(30) Gütlich, P.; Bill, E.; Trautwein, A. X., *Mossbauer Spectroscopy and Transition Metal Chemistry. Fundamentals and Applications.* Springer-Verlag Berlin Heidelberg: **2011**.
(31) Neese, F. Software update: the ORCA program system, version 4.0. *WIREs Comput. Mol. Sci.* **2018,** *8*, e1327.
(32) Gu, Y.; Kar, T.; Scheiner, S. Fundamental Properties of the CH···O Interaction: Is It a True Hydrogen Bond? *J. Am. Chem. Soc.* **1999,** *121*, 9411-9422.
(33) Batsanov, S. S. Van der Waals Radii of Elements. *Inorganic Materials* **2001,** *37*, 871-885.
(34) (a) Grünert, G. C.; Reiman, S.; Spiering, H.; Kitchen, J. A.; Brooker, S.; Gütlich, P. Mixed Spin - State [HS - LS] Pairs in a Dinuclear Spin - Transition Complex: Confirmation by Variable - Temperature ^{57}Fe Mössbauer Spectroscopy. *Angew. Chem., Int. Ed.* **2008,** *47*, 2997-2999; (b) Griffin, M.; Shakespeare, S.; Shepherd, H. J.; Harding, C. J.; Letard, J.-F.; Desplanches, C.; Goeta, A. E.; Howard, J. A. K.; Powell, A. K.; Mereacre, V.; Garcia, Y.; Naik, A. D.; Mueller-Bunz, H.; Morgan, G. G. A Symmetry-Breaking Spin-State Transition in Iron(III). *Angew. Chem., Int. Ed.* **2011,** *50*, 896-900, S896/1-S896/17; (c) Lennartson, A.; Bond, A. D.; Piligkos, S.; McKenzie, C. J. Four - Site Cooperative Spin Crossover in a Mononuclear Fe^{II} Complex. *Angew. Chem., Int. Ed.* **2012,** *51*, 11049-11052.(d) Murnaghan, K. D.; Carbonera, C.; Toupet, L.; Griffin, M.; Dîrtu, M. M.; Desplanches, C.; Garcia, Y.; Collet, E.; Letard, J. -F.; Morgan, G. G. Spin-State Ordering on One Sub-lattice of a Mononuclear Iron(III) Spin Crossover Complex Exhibiting LIESST and TIESST. *Chem. Eur. J.* **2014**, *20*, 5613-5618. (e) Fitzpatrick, A. J.; Trzop, E.; Muller-Bunz, H.; Dîrtu, M. M.; Garcia, Y.; Collet, E.; Morgan, G. G. Electronic vs. structural ordering in a manganese(III) spin crossover complex. *Chem. Commun.* **2015**, *51*, 17540-17543.
(35) Garcia, Y.; Robert, F.; Naik, A. D.; Zhou, G.; Tinant, B.; Robeyns, K.; Michotte, S.; Piraux, L. Spin Transition Charted in a Fluorophore-Tagged Thermochromic Dinuclear Iron(II) Complex. *J. Am. Chem. Soc.* **2011,** *133*, 15850-15853.
(36) Zhuang, J. Z.; Tao, J.-Q.; Yu, Z.; Dun, C.-Y.; Liu, Y.-J.; You, X.-Z. A stacking spin-crossover iron(II) compound with a large hysteresis. *J. Chem. Soc., Dalton Trans.* **1998**, 327-328.
(37) Lagarec, K.; Rancourt, D. G. Recoil, Mössbauer Spectral Analysis software for Windows 1.0, Department of Physics, University of Ottawa, **1998**.
(38) Sheldrick, G. A short history of SHELX. *Acta Crystallographica Section A* **2008,** *64*, 112-122.
(39) Weigend, F. Accurate Coulomb-fitting basis sets for H to Rn. *Phys. Chem. Chem. Phys.* **2006,** *8*, 1057-1065.
(40) Pantazis, D. A.; Chen, X.-Y.; Landis, C. R.; Neese, F. All-Electron Scalar Relativistic Basis Sets for Third-Row Transition Metal Atoms. *J. Chem. Theory Comput.* **2008,** *4*, 908-919.
(41) Wüllen, C. v. Molecular density functional calculations in the regular relativistic approximation: Method, application to coinage metal diatomics, hydrides, fluorides and

chlorides, and comparison with first-order relativistic calculations. *J. Chem. Phys.* **1998,** *109*, 392-399.
(42) (a) Grimme, S.; Ehrlich, S.; Goerigk, L. Effect of the damping function in dispersion corrected density functional theory. *J. Comp. Chem.* **2011,** *32*, 1456-1465; (b) Grimme, S.; Antony, J.; Ehrlich, S.; Krieg, H. A consistent and accurate ab initio parametrization of density functional dispersion correction (DFT-D) for the 94 elements H-Pu. *J. Chem. Phys.* **2010,** *132*, 154104.
(43) Pinter, B.; Chankisjijev, A.; Geerlings, P.; Harvey Jeremy, N.; De Proft, F. Conceptual Insights into DFT Spin - State Energetics of Octahedral Transition - Metal Complexes through a Density Difference Analysis. *Chem. - Eur. J.* **2017,** *24*, 5281-5292.

For Table of Contents Only

The combination between electronic substituent effect isopropyl acetate group and C-H···O interactions provides relatively high cooperativity, which leads to an abrupt SCO behavior in [Fe(H_2Bpz_2)$_2$(***i*-PrObpydc**)] **.**